MICROCOPY RESOLUTION TEST CHART

⑫ **LEVEL** Ⅲ

AD-E300 661

DNA 4766F

SCINTILLATOR RESPONSE CHARACTERISTICS TO LOW-ENERGY X-RAYS

ADA081720

Lockheed Palo Alto Research Laboratory
3251 Hanover Street
Palo Alto, California 94304

30 November 1978

Final Report for Period January 1978—November 1978

CONTRACT No. DNA 001-78-C-0109

APPROVED FOR PUBLIC RELEASE;
DISTRIBUTION UNLIMITED.

DTIC
SELECTE**D**
MAR 1 2 1980

B

DDC FILE COPY

Prepared for
Director
DEFENSE NUCLEAR AGENCY
Washington, D. C. 20305

80- 3 1 180

(19) REPORT DOCUMENTATION PAGE	READ INSTRUCTIONS BEFORE COMPLETING FORM

1. REPORT NUMBER	2. GOVT ACCESSION NO.	3. RECIPIENT'S CATALOG NUMBER
DNA 4766F HI-E300 661		

4. TITLE (and Subtitle)
SCINTILLATOR RESPONSE CHARACTERISTICS TO LOW-ENERGY X-RAYS

5. TYPE OF REPORT & PERIOD COVERED
Final Report for Period Jan 78 — Nov 78

6. PERFORMING ORG. REPORT NUMBER
LMSC/D630965

7. AUTHOR(s)
J. G. Pronko
T. R. Fisher
L. F. Chase

8. CONTRACT OR GRANT NUMBER(s)
DNA 001-78-C-0109

9. PERFORMING ORGANIZATION NAME AND ADDRESS
Lockheed Palo Alto Research Laboratory
3251 Hanover Street
Palo Alto, California 94304

10. PROGRAM ELEMENT, PROJECT, TASK AREA & WORK UNIT NUMBERS
Subtask J11AAXAX004-40

11. CONTROLLING OFFICE NAME AND ADDRESS
Director
Defense Nuclear Agency
Washington, D.C. 20305

12. REPORT DATE
30 November 1978

13. NUMBER OF PAGES
50

14. MONITORING AGENCY NAME & ADDRESS(if different from Controlling Office)

15. SECURITY CLASS (of this report)
UNCLASSIFIED

15a. DECLASSIFICATION/DOWNGRADING SCHEDULE

16. DISTRIBUTION STATEMENT (of this Report)

Approved for public release; distribution unlimited.

17. DISTRIBUTION STATEMENT (of the abstract entered in Block 20, if different from Report)

18. SUPPLEMENTARY NOTES

19. KEY WORDS (Continue on reverse side if necessary and identify by block number)
High Speed X-Ray Streak Camera
Scintillator Response
Low-Energy X-Rays
Emission Wavelength

20. ABSTRACT (Continue on reverse side if necessary and identify by block number)
The response of the organic scintillator, NE111, to subnanosecond pulses of low-energy x-rays was studied as a function of fluorescence emission wavelength. The characteristic emission spectra of a matrix of NE111 doped with benzophenone, acetophenone, and piperidine each at concentrations of 0, 2, 5 and 10 percent were measured using low-energy DC-electron excitation and a Mark V, 0.5-m, Jarrell-Ash spectrograph. In addition, absorption spectra covering the region of 300 to 500 nm were accumulated using a Cary Recording

20. ABSTRACT (Continued) $(< approximately)$ $(< \cdots =$

Spectrometer (Model 14). A series of response measurements were performed in which the emission spectrum incident on a detection system was filtered by selected narrow band $(\leq 10$ nm) filters. The scintillator fluorescence was excited by 0.2-ns pulses of x-rays $(\leq 2$ keV) produced in a laser plasma with the LPARL Nd:glass laser facility. Fast-time response measurements were performed using an S20 streak camera. In addition, the ratio of the integral of the emitted fluorescence in the first 8 ns to the integral out to 1 s was determined as a function of emission wavelength. In neither of these experiments was it possible to produce relevant changes in the scintillator response by the introduction of filters. Studies similar to those performed previously at LPARL on the non-linear, saturation properties of organic scintillators to low-energy x-rays were continued at higher x-ray fluences. It was found that the scintillator responded linearly to low-energy x-rays ($E_x \leq 2$ keV) up to the maximum irradiance achieved for a 0.2-ns pulse. For this case the 10-percent nonlinearity point was set at ≥ 85 mJ/cm^2-ns. The highlights of a similar experiment are presented for x-ray pulses in the region of 6-ns width. In that case, it was found that the 10-percent nonlinearity point was at an irradiance of ~ 2 mJ/cm^2-ns.

PREFACE

Presented herein is the draft final report submitted to the
Defense Nuclear Agency (DNA) by the Lockheed Palo Alto
Research Laboratory (LPARL) for contractual research
performed under Contract DNA001-78-C-0109 for the
period January 1978 to November 1978.

DTIC
S ELECTE **D**
MAR 1 2 1980

B

1

TABLE OF CONTENTS

LIST OF ILLUSTRATIONS

4

TABLES

Section 1
INTRODUCTION

A recent investigation (Ref. 1) by Lockheed Palo Alto Research Laboratory (LPARL) into the response characteristics of organic scintillators to low-energy x rays has revealed much in the way of information necessary for optimum use of these scintillators in the detection of short, intense bursts of low-energy x rays. The study was concerned with a variety of fluorescence properties, such as risetime, response width, short- and long-term decay components, and saturation effects of NE102, NE111 and doped NE111 scintillators to x rays with energies $\leq$ 2 keV. Although this investigation was rather comprehensive in scope, there remained a number of aspects which needed to be expanded upon in order to utilize these organic scintillators most effectively in detecting intense bursts of low-energy x rays.

The LPARL investigation (Ref. 2) had revealed that doping the organic scintillator with the aromatics, benzophenone, acetophenone, and piperidine resulted in a vast improvement in the short-term time response. However, this was achieved at the expense of total light output. It is not clear what the mechanism is that is responsible for the improvement in temporal response or for the loss of fluorescence light output. If, however, the response could be improved without the attendant decrease in light output, the doped scintillators could be used far more effectively. Such an abstraction can be carried still further to include the possibility of reducing, by some suitable convenient technique, the ratio of the long-term time component to the total light output.

One possibility is to take advantage of the fact that the emission spectrum of NE111 is fairly broad and consists of a number of components. It is reasonable to expect that an observed response characteristic could be suitably altered by detecting only selected portions of the output emission spectrum. Consequently, one aim of the present investigation was to measure these response characteristics as a function of fluorescence emission wavelength to determine whether the observed response could be improved through selective filtering of the NE111 emission spectrum.

7

Another important aspect is that of scintillator nonlinear effects. The results of the previous investigation (Ref. 1) indicate that for a 0.2-ns pulse of x rays ($E_x \leq 2$ keV), no nonlinear effects could be measured in the response of NE102 and NE111 for irradiances ≤ 15 mJ/cm^2-ns. These measurements, which provide the only data available regarding nonlinear effects at high x-ray doses, provide no indication of scintillator saturation or signal nonlinearity at irradiances three orders of magnitude greater than the levels previously accepted as being free from such effects. Earlier estimates were based on a limiting level of approximately 2500 ergs/g-ns.

Studies (Refs. 2, 3, and 4) have been made of the nonlinear response of the organic scintillator NE102 using high-energy electrons. These data suggest that the point at which nonlinearity was observed was dependent not only on total dose but on dose rate as well. Their studies did not include pulse widths less than 6 ns, but an extrapolation of these results to the 0.2-ns width used in the LPARL experiments indicates that the x-ray measurements (when normalized to energy deposited/unit volume) showed no effects of nonlinearity at levels that were two orders of magnitude higher than that which would be expected from the extrapolation of the electron data (Ref. 2). In view of this apparent discrepancy, it is important to extend the saturation measurements to include x-ray pulse widths comparable to those used in collecting the electron data as well as to cover the region between the LPARL 0.2-ns data and the electron 6-ns data. The results of such measurements would eliminate the need for making gross extrapolations in defining a particular saturation level as well as aid in determining the validity of the intercomparison between the x-ray and electron saturation data.

The objectives of the present investigation were manifold. The first was to measure emission and absorption properties of NE111 so as to be able to make sound choices in the method of attempting to improve the scintillator response properties without producing some of the less desirable effects associated with scintillator doping. Such studies involved the principles of emission and absorption spectrometry. The results are presented in Section 2.

The second objective was to experimentally attempt to improve scintillator response by using selective filtering based on the input of the previous section. The results of this portion of the investigation are presented in Section 3.

The third objective was to extend the scintillator nonlinear response studies to irradiances higher than previously used (Ref. 2) and, if possible, to longer pulse widths than those previously used. The former was accomplished; however, it was not possible, on a best efforts basis, to include the latter goal in the present investigation. Nonetheless, data of this nature, which represent the highlights of data obtained in an alternate LPARL study (Ref. 5), shall be reviewed in this report. The results of this third objective are presented in Section 4. Summarized in Section 5 are the results of this investigation and the conclusions derived therefrom.

Section 2
SCINTILLATOR SPECTRAL PROPERTIES

2.1 SCINTILLATOR EMISSION SPECTRA

Previous measurements (Ref. 6) of organic scintillator emission spectra indicated that the spectra are rather broad and probably contain a number of decay components. Since a component in an emission spectrum may be associated with the properties of a particular excited state or system, it is possible that a measurable scintillator response characteristic might be favorably altered by detecting only selected portions of the output fluorescence spectrum. To have a guide as to what wavelength filters should be used in an experiment of this nature, it is necessary to measure, at least, the gross features of the emission spectra. Nuclear Enterprises, Inc. present (Ref. 6) the emission spectra of a number of important organic scintillators, including NE102 and NE111. However, there are no data available on the emission spectra of the doped versions of NE111. Consequently, it was necessary to make these measurements.

Originally, it was proposed that these emission spectra measurements be made using a dc x-ray generating machine, such as a Henke Tube. However, the difficulty in coupling an x-ray generating system to the spectrometer, as well as the low-light yield (in particular for doped samples) that resulted from this kind of excitation, precluded the use of such a concept. Instead, it was felt that a high-current, low-energy electron gun in a close-coupled configuration would be more suited to making measurements of this nature. The high current concept would eliminate the intensity difficulty, while the low-energy ($\lesssim$ 10 keV) electrons (as opposed to γ rays or MeV electrons) would more closely resemble low-energy x rays. Since the emission spectra might possibly be dependent on the energy or mode of excitation, this latter point is important.

The experimental arrangement for recording scintillator fluorescence spectra is shown schematically in Figure 1. Bombardment with electrons from a 20 kV e-gun was used to excite the fluorescence. The e-beam was focused by a magnetic solenoid lens

and directed by a pair of orthogonal magnetic steering coils to arrive at the scintillator which was situated at the end of a one-meter flight path. Each scintillator was fabricated in the form of a disk 4.5 cm in diameter by 3 mm thick, and the vacuum seal at the end of the beam tube was made directly to the scintillator surface by means of an o-ring. This design facilitated close coupling between the scintillator and the entrance slit of the Mark V, 0.5-m, Jarrell-Ash spectrograph which provided the wave-length dispersion for the analysis of the scintillator light output. This spectrograph has an automatic motor drive which rotates the grating to provide a linear scan of the spectral region under study.

A 1000 $\overset{\circ}{A}$ layer of aluminum was evaporated on the scintillator side toward the e-beam to suppress background light from the filament and to provide a conducting path for the escape of charge from the scintillator surface.

In initial tests, the output from the EMI 9558 phototube was connected directly to a Keithley Model 640 electrometer. With this arrangement, 1 to 5 $\mu a/cm^2$ of electron current was required to obtain spectra of good statistical quality from an undoped NE102 or NE111 scintillator. Since significant deterioration in scintillator light output with time was already evident at this bombardment current, and the light output from doped scintillators was known to be greatly reduced in some cases, it was necessary to devise some means to achieve a significant increase in detection sensitivity. This was accomplished by adding a third magnetic steering coil driven by a 4-kHz sinusoidal current from an audio amplifier. The audio amplifier input was furnished by the internal reference signal from a PAR model JB-5 lock-in amplifier, and the output from the EMI 9558 phototube was fed back into the lock-in amplifier for in-phase signal detection. This arrangement yielded approximately 3 orders of magnitude improvement in sensitivity with a 1-s integrating time constant on the lock-in amplifier.

Using the final experimental arrangement shown in Figure 1, it was possible to record spectra for the low-yield, doped scintillator samples with an average electron current of <50 na illuminating about 1 cm^2 of scintillator surface. The usual scan speed was 500 $\overset{\circ}{A}$/min, the maximum speed available. This scan speed was chosen to minimize the effects of slow drifts in beam current on the spectrum shape. Several
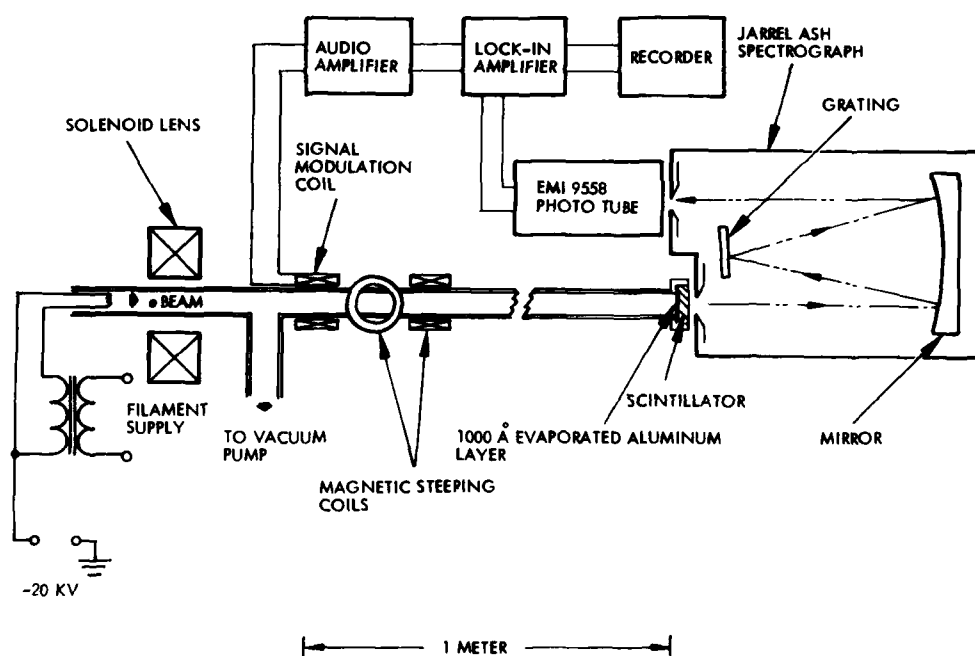
Figure 1. A schematic representation of the experimental configuration for recording fluorescence spectra.

12

spectra were taken for each scintillator sample to average out the effects of such drifts. The entrance slit width was set at 2 mm which corresponds to a spectrograph resolution of about 3 nm, a value negligible compared to the scale of the observed structure.

The spectrometer calibration was checked using spectral lines from an Hg source and was found to be within 0.2 nm. All spectra collected were digitized using an x-y table and then corrected for the response of the system. The system response was obtained by folding the manufacturer's efficiency data for the S20 photomultiplier and the grating. The grating had 1180 grooves/mm, a blaze angle of 17.2 deg, and a blaze wavelength of 500 nm.

Figures 2, 3, and 4 illustrate the results obtained with this system for NE111 and NE111 doped with 1, 2, 5, and 10 percent benzophenone, acetophenone, and piperidine. Figure 5 illustrates the equivalent spectrum obtained for NE102. All of the above spectra include a correction for the phototube and grating response.

The area of each spectral distribution represents the total light output and is normalized, using the curves presented in a previous LPARL report (Ref. 1), relative to the 0 percent spectrum. The measured spectra for NE102 and NE111 agree qualitatively with past results (Ref. 6). As illustrated in Figures 2 through 4, the undoped NE111 emission spectrum appears to have two major components. The structure at the shorter wavelength diminishes in intensity with increasing levels of dopant and disappears entirely at a benzophenone doping level of 10 percent. The implications drawn from these measurements are discussed in the following sections.

2.2 SCINTILLATOR ABSORPTION MEASUREMENTS

The results of the previous subsection indicate that for highly doped scintillators the light emitted at the short wavelengths are strongly attenuated relative to the remainder of the spectrum. In an attempt to further understand this effect, an experiment was designed to measure the self-absorption of the doped scintillators over the frequency range of the emitted scintillator light.

A Cary Recording Spectrophotometer (Model 14) formed the basis of the experiment. This is shown schematically in Figure 6. This model employs a double monochromator
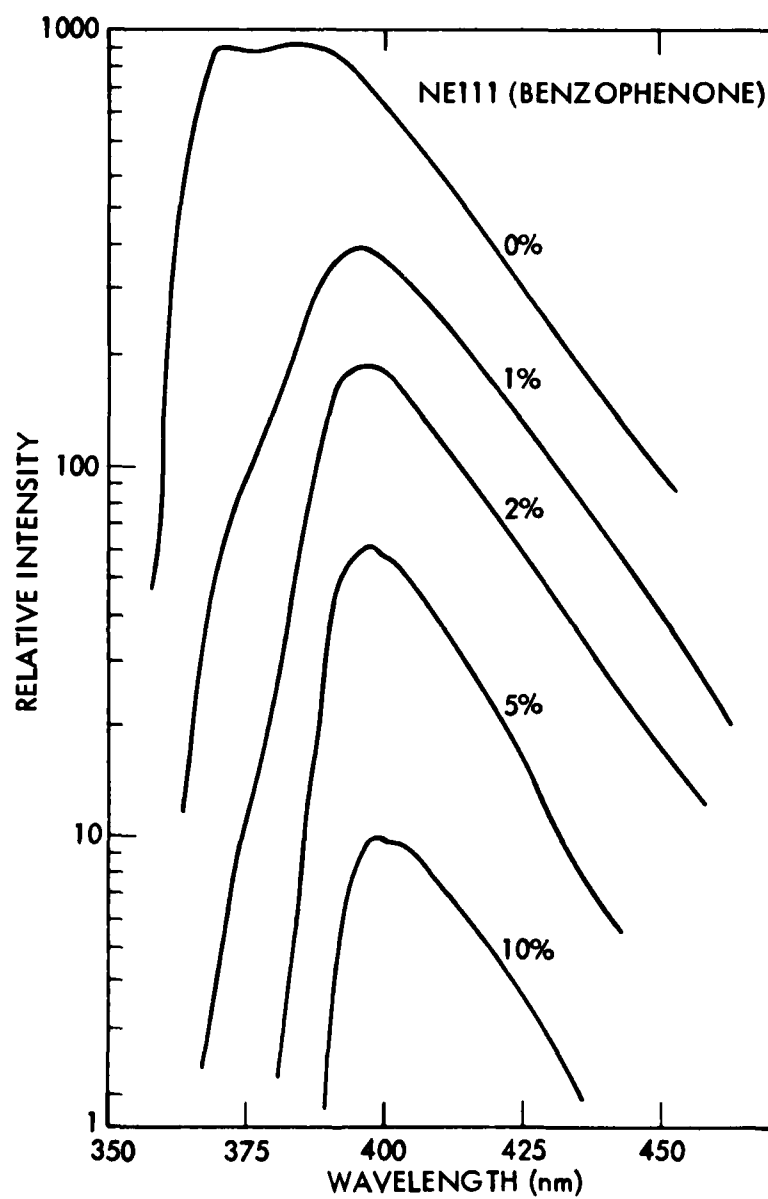
Figure 2. The NE111 scintillator emission spectra as measured
in the present experiment for various doping levels of
benzophenone. The area of each spectral distribution
represents the total light output and is normalized
relative to the 0 percent spectrum. These spectra in-
clude a correction for the system response.

14
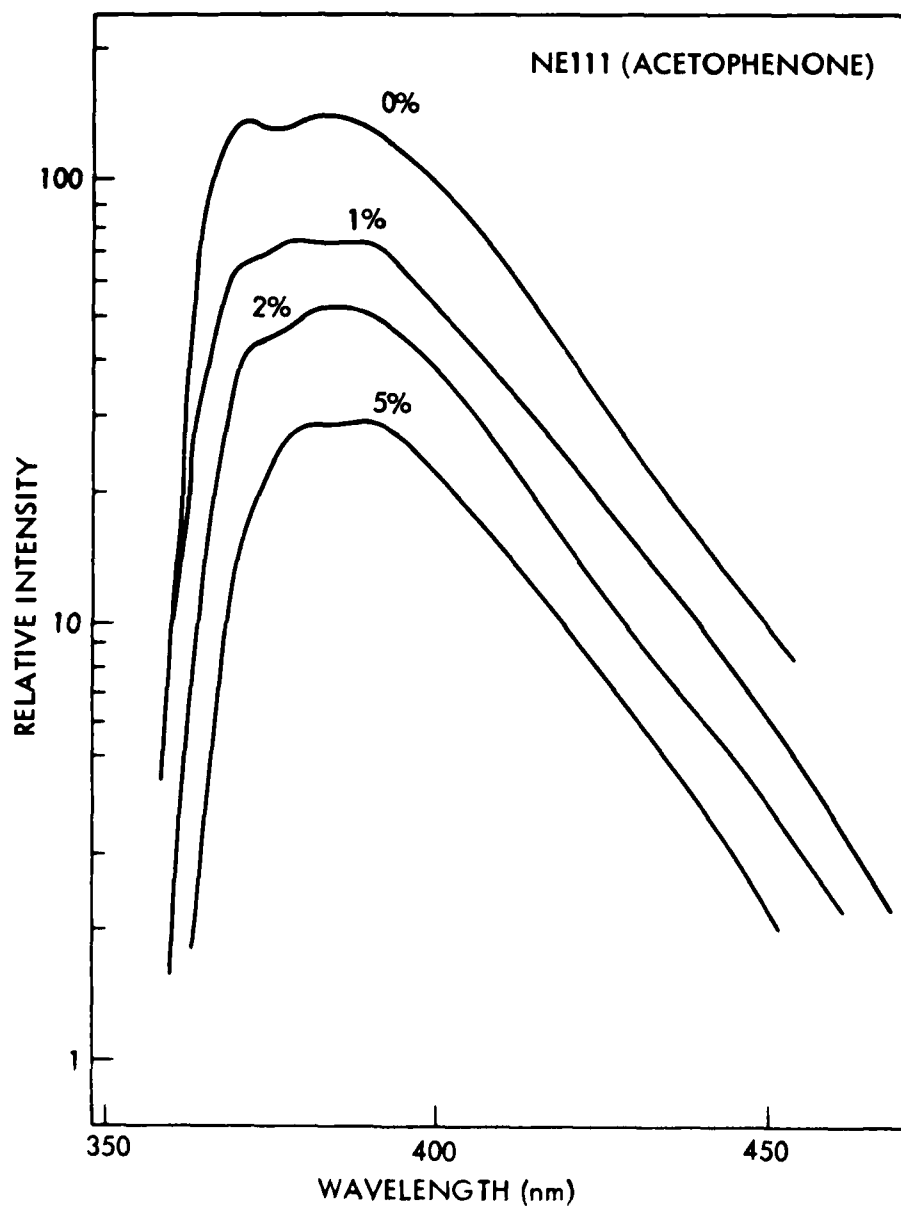
Figure 3. The NE111 scintillator emission spectra as measured in the present experiment for various doping levels of acetophenone. The area of each spectral distribution represents the total light output and is normalized relative to the 0-percent spectrum. These spectra include a correction for the system response.
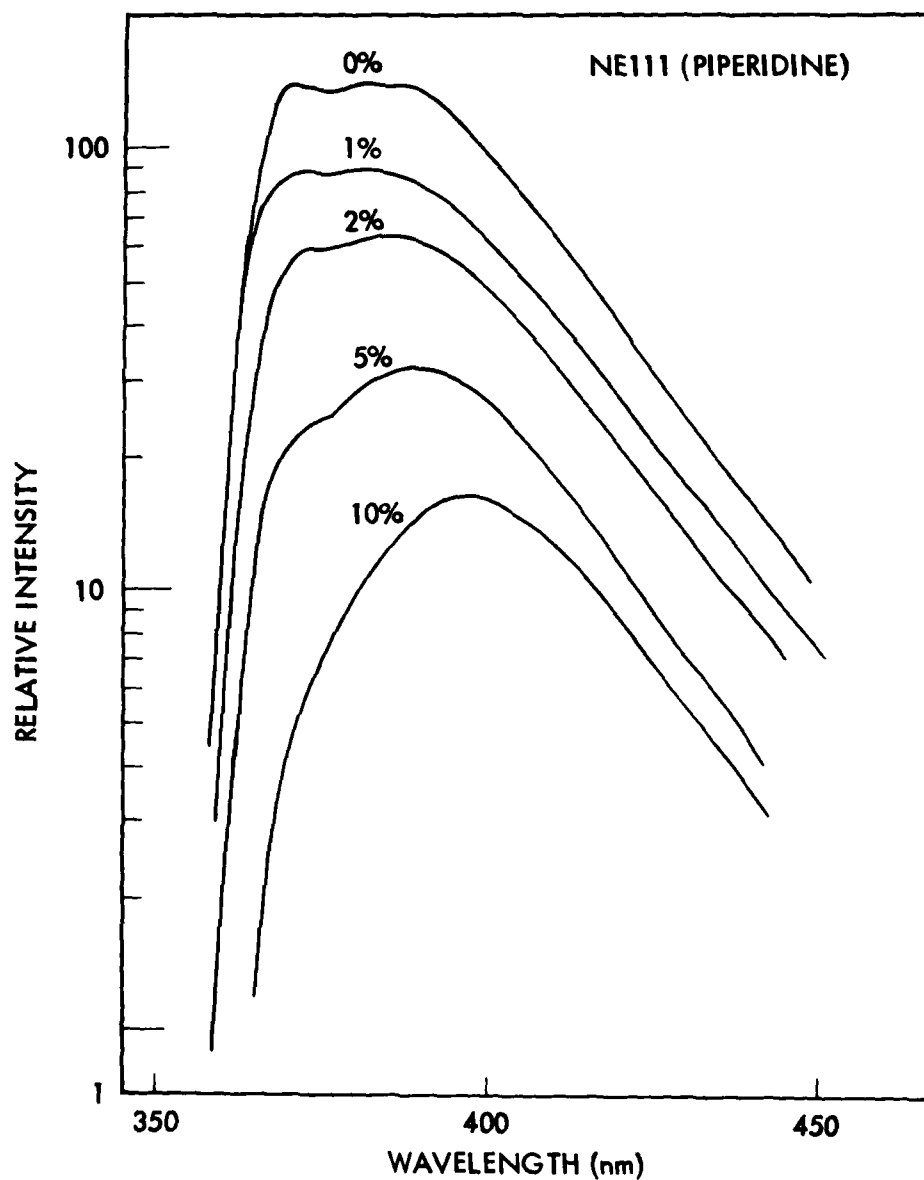
Figure 4. The NE111 scintillator emission spectra as measured in the present experiment for various doping levels of piperidine. The area of each spectral distribution represents the total light output and is normalized relative to the 0-percent spectrum. These spectra include a correction for system response.

16
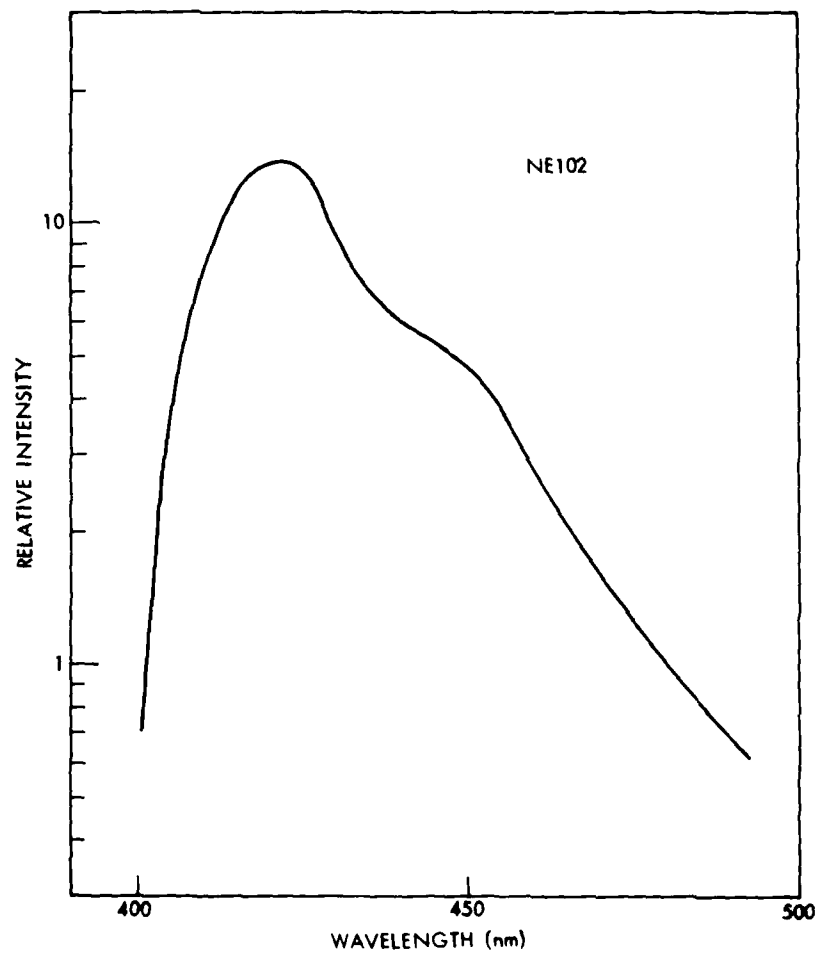
Figure 5. The NE102 scintillator emission spectrum as measured
in the present experiment. The spectrum has been cor-
rected for system response.
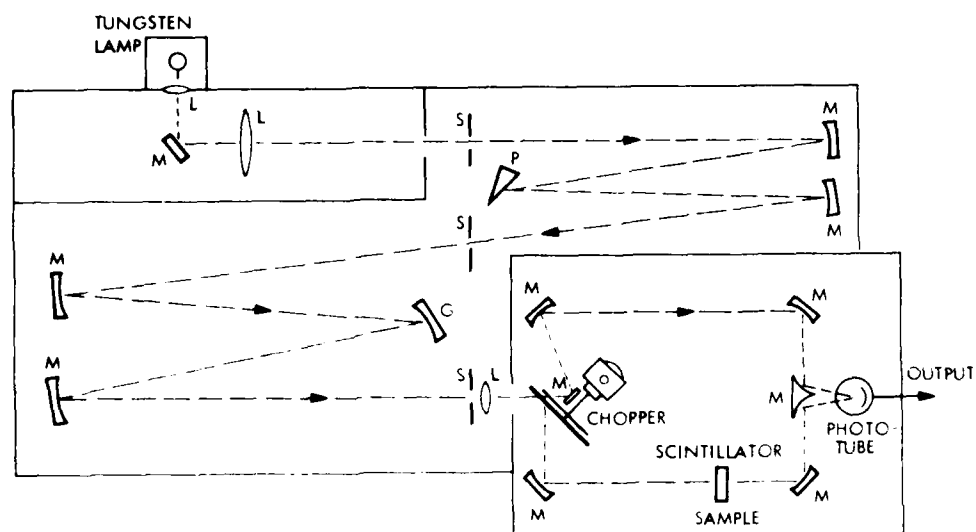
Figure 6. A schematic representation of the experimental configuration using a Cary Recording Spectrophotometer for measuring the scintillator absorption spectra. See text for further details.

for the tungsten light source consisting of a 30-deg fused silica prism (P) in series with a 600 line/mm echelette grating (J) and the appropriate mirrors (M) and slits (S). The prism and grating are synchronously rotated in order to scan the spectral region of interest. The resolving power for these wavelengths is approximately 0.1 nm. The monochromatic light from the exit slit is alternately sent through the sample and reference systems at 30 cps by means of a semicircular mirror and rotating chopper system. The light is then recombined at the phototube and sampled by the electronic circuitry at a rate synchronous with the chopper. A signal is generated by the final circuitry which is proportional to the difference between the two signals. This then provides a normalized light absorption measurement of the scintillator sample.

The results of these measurements are illustrated in Figure 7. The vertical axis represents the absolute value of the absorption optical density. Although not shown in the figure, these curves continue on to optical densities ≥ 2. In the case of NE111 doped with acetophenone, it appears as though the absorption edge does not change in wavelength as the percentage of dopant is increased. This does not appear to be the case for benzophenone; in fact, the absorption edge shifts to longer wavelengths as the percentage of dopant is increased. This shift can be correlated with the relative attenuation of portions of the emission spectra shown in Figure 6. The emission spectra for NE111 doped with acetophenone have the least change in spectral shape as the percentage of dopant is increased and corresponds to what is observed in the absorption data of Figure 7. The data for piperidine lie somewhere between these two extreme cases.
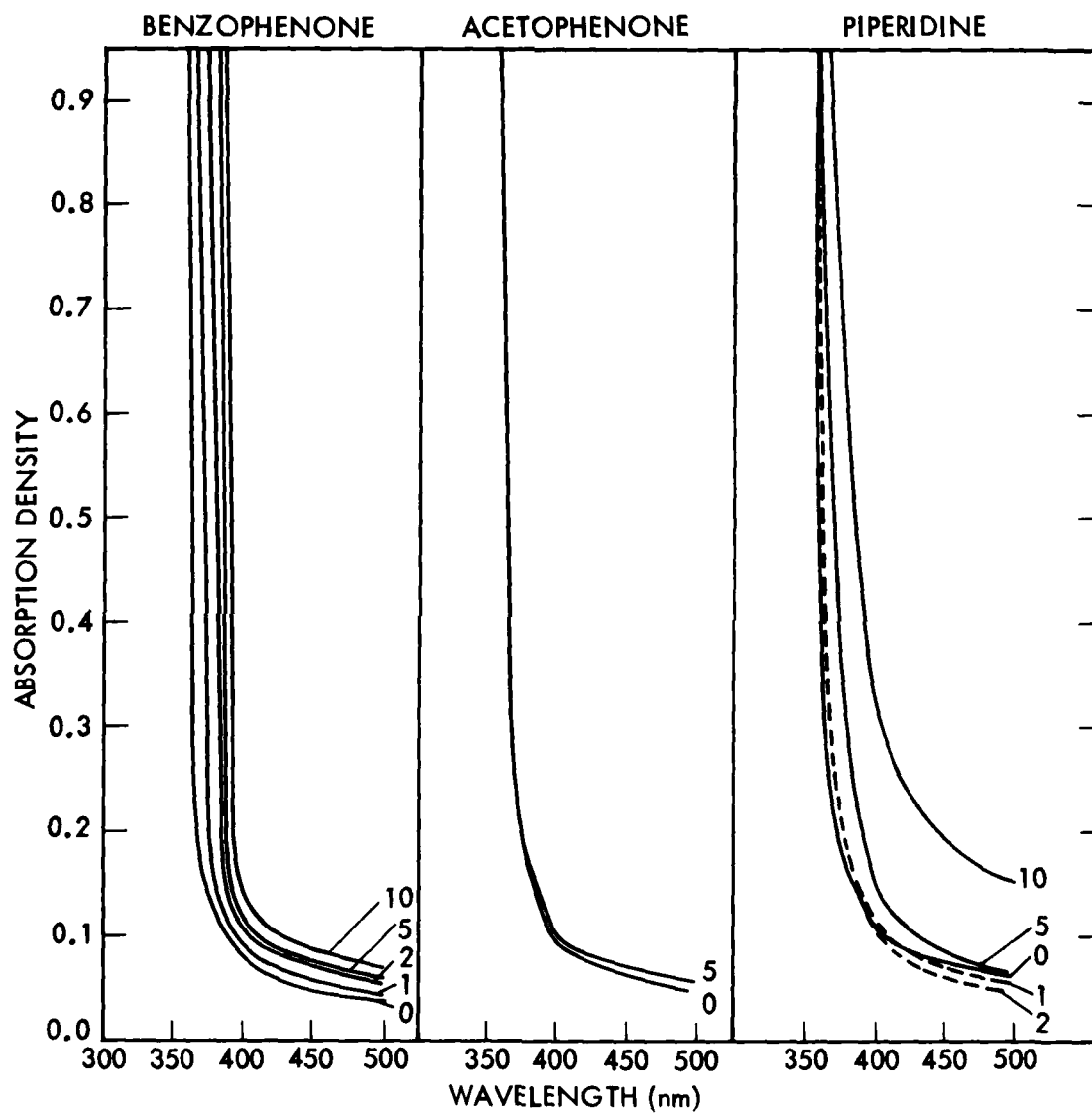
Figure 7. A plot of absorption optical density as a function of wavelength for doped NE111. The number associated with each curve represents the percentage of dopant. For the case of acetophenone, the curves for 1 and 2 percent fall between the two illustrated.

Section 3
SELECTIVE FILTERING STUDIES

3.1 FAST TIME RESPONSE

From the scintillator emission spectra measured in Section 2, it was found that for
the highly doped scintillators, the light emitted at the short wavelengths ($\sim$ 375 nm)
was attenuated or possibly shifted to longer wavelengths. This was particularly strik-
ing in the case of benzophenone. In addition, the absorption measurements imply that
for the case of benzophenone, there appears to be a shift of the absorption edge to
longer wavelengths as the percentage of dopant is increased. This suggests the possi-
bility that the mechanism whereby the time response is improved could result merely
from the in situ absorptive nature of benzophenone. If this be the case, then it might
not be necessary to dope the NE111; but rather, the same results could be accomplished
through the use of filters external to the scintillator. To test this hypothesis, an ex-
periment was designed in which the temporal response was measured as a function of
emission wavelength.

The experimental arrangement for these studies is illustrated in Figure 8. The streak
camera was positioned 40 cm from the scintillator, and the fluorescent light was focused
onto the image slits via an air path and the streak camera relay optics. The narrow-
band filters were positioned in this air path at a distance of 16 cm from the target.
The scintillator samples were positioned against a 0.0254-mm beryllium vacuum
window, which was glued around a 0.645-cm-diameter hole at the end of an aluminum
tube. This tube protruded through the side of the vacuum chamber allowing the scin-
tillator to be positioned as close as 1.5 cm from the target spot. The target was a
planar piece of copper oriented at 45 deg to the laser beam. The laser oscillator
cavity was operated with a 2-mm etalon, producing laser pulses in the region of 200 ps.
The flux incident on the scintillator was nominally 50 μJ/cm^2 of x rays in the energy

TARGET CHAMBER

Cu TARGET

1.06-µM LASER BEAM

X RAYS

Be VACUUM, LIGHT SEAL
AND SCINTILLATOR

NARROW
BAND
FILTER

LIGHT
SHIELD

STREAK
CAMERA

INTENSIFIER

RECORDING
CAMERA
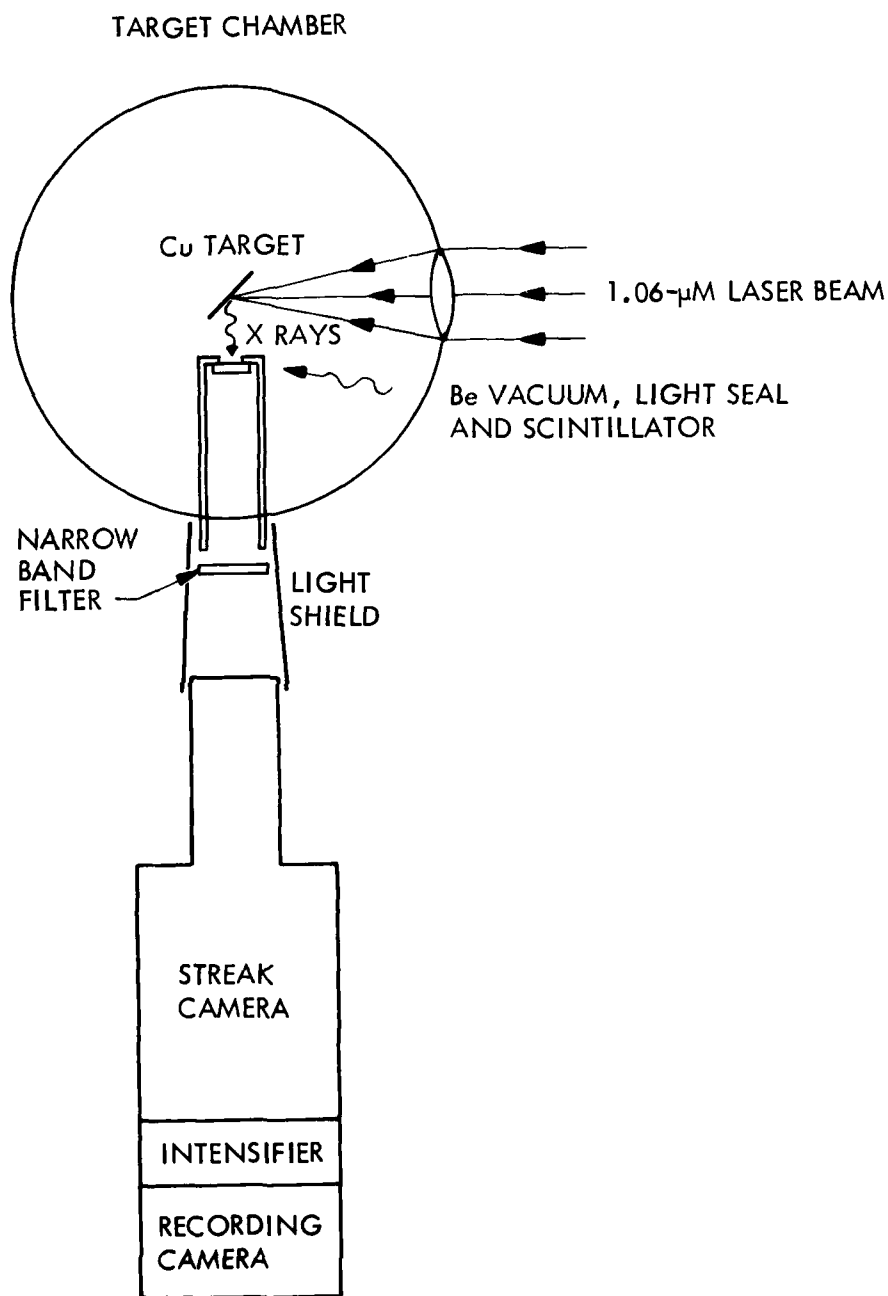
Figure 8. An experimental arrangement used in the present
investigation for measuring the fast-time charac-
teristics of scintillator fluoresence as a function
of emission wavelength.

region of 0.7 to 2 keV. An XRD detector served as a monitor at a position 45 deg to the incident beam. The scintillator samples were disks nominally 2.5 cm in diameter and 0.32 cm thick.

The filters used for this experimental effort as well as the experiment described in the following section was from a set of 2.54 × 2.54 cm bandpass interference filters covering the wavelength region of 350 nm to 500 nm in steps of 10 nm. The filters consisted of the 3-cavity configuration manufactured by Ditric Optics Inc. The bandwidth and transmission of the available filters were center wavelength dependent and varied from 6.5 to 11 nm and 30 to 50 percent, respectively.

The streak camera used in the present investigation is an Imacon 675 manufactured by Hadland Photonics Limited and included an S20 cathode and a Channeltron electron multiplier array (CEMA) intensifier system for signal readout. The streak signal at the output of the intensifier was recorded on Polaroid 410 film or Kodak Royal X Pan film (4166). The data recorded with the latter film could be read with a microdensitometer for subsequent analysis.

Data were collected at a sweep speed which corresponded to 390 ps/mm on the film at the streak camera output. This is not the fastest available rate; rather, it is a compromise value in order to optimize both intensity and time resolution. The time axis had been calibrated in a previous experiment and can be found in Ref. 1, where the intensity axis was also calibrated, using the step wedge filter concept. However, that calibration was for a set of conditions different from the present setup (in particular sweep speed) and consequently could not be used for a quantitative analysis of the data. Since a new calibration was not performed for the present experimental configuration, a qualitative analytical approach was deemed more suitable. Examples of such an analysis are given in Figure 9.

The top curve illustrates a densitometer trace of film data taken with undoped NE111 using no narrowband filter. The bottom curve illustrates a densitometer trace of film data taken with NE111 doped with 10 percent benzophenone. From Ref. 1 it is known that the latter scintillator yielded the narrowest pulse width of all samples in the available scintillator matrix. The vertical axis is a relative scale of optical density,
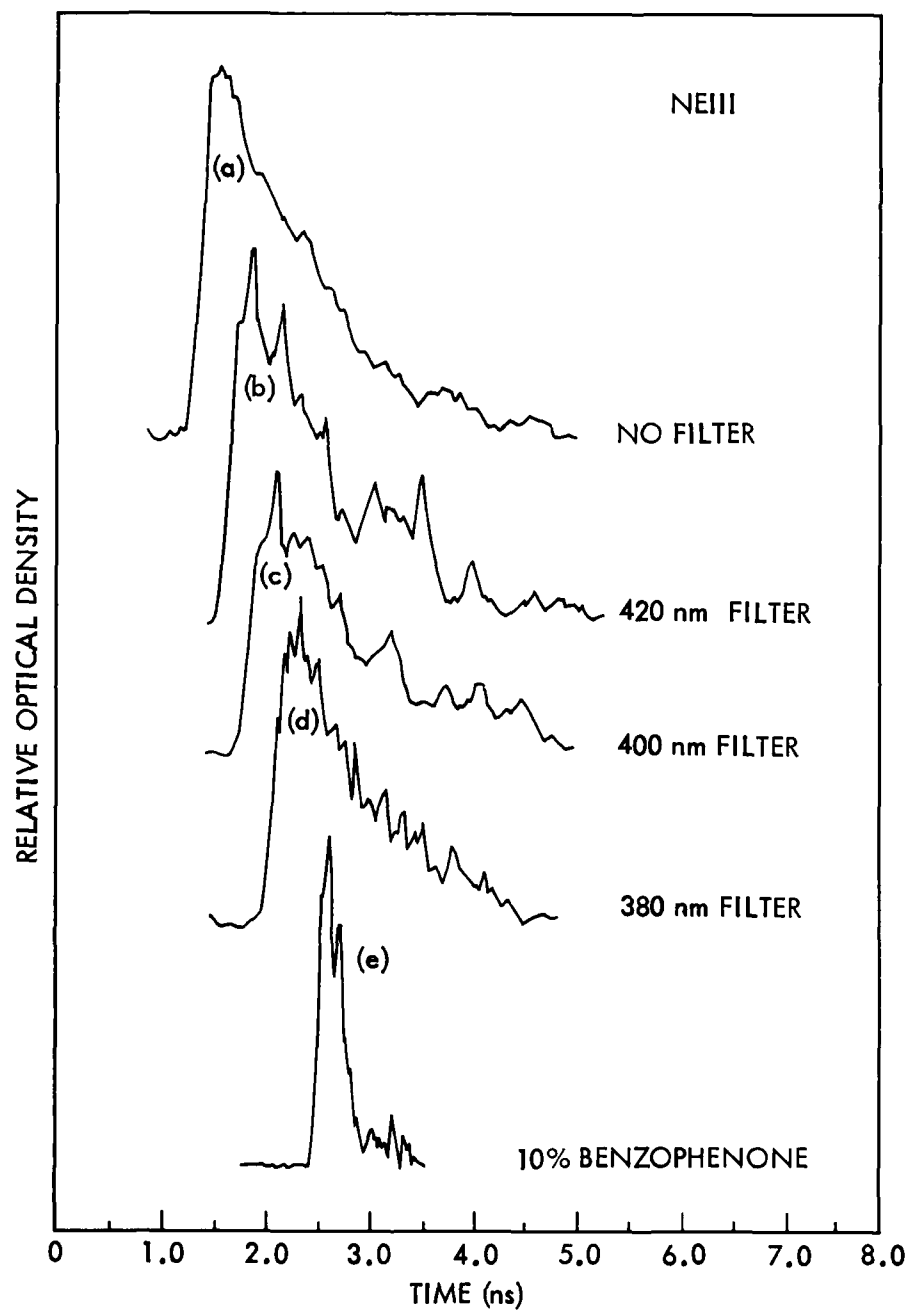
Figure 9. Densitometer traces of streak camera film data. The vertical axis is a relative scale of optical density and the curves are not normalized to each other.

24

and none of the curves presented in Figure 8 is normalized with respect to the others. The widths represented by these curves are in qualitative agreement with the previous experiment of Ref. 1. No quantitative analysis of the data was attempted because of the lack of the proper linearizing calibration curve.

The three remaining curves presented in Figure 8 are densitometer examples of the streak traces obtained with three different wavelength filters. These filters were selected on the basis of their center wavelength and represented three definitive regions of interest in the spectra of Figure 2.

The wavelength in the vicinity of 380 nm represents that region which appears to be greatly attenuated (relative to the remaining wavelength) as the concentration of doping material is increased. The wavelength of 400 nm represents the peak of the region that appears to be attenuated the least. The data using the 420-nm filter represents a point in the low-energy tail of the spectrum.

The widths of the curves b, c, and d are comparable to the widths of the undoped NE111 data. Within the statistical accuracy of the data, no difference in width could be seen between any of the data collected under conditions a through d.

3.2 LONG-TERM DECAY STUDIES

From the results presented in Section 2, it is seen that the NE111 emission spectrum is composed of at least two major components, one of which diminishes in intensity as the percentage of dopant is increased. Since it has been shown in a previous report (Ref. 1) that the fast time response improves with an increase in dopant concentration, it is reasonable to believe that these longer decay components might be associated with the diminishing structure at the high-energy end of the spectrum. With this in mind, an experiment was designed whereby the ratio of the integral of the fluorescence emission in the first 8 ns to the total integral (< 1 s), as a function of emission wavelength, was determined. The experimental arrangement is shown schematically in Figure 10. The x rays were generated with a Cu target at a pulse width of approximately 6.5 ns. The signal from a scintillator–photodiode system, in which filters of known bandpass can be placed, were routed through a power splitter, into

TARGET CHAMBER

TARGET

LASER LIGHT

X-RAYS

Be FILTER
SCINTILLATOR
NOTCH FILTER
LIGHT PIPE AND COLLIMATOR
DIODE

POWER DIVIDER

BLOCKING
CAPACITOR

TEKTRONIX
7904
OSCILLOSCOPE
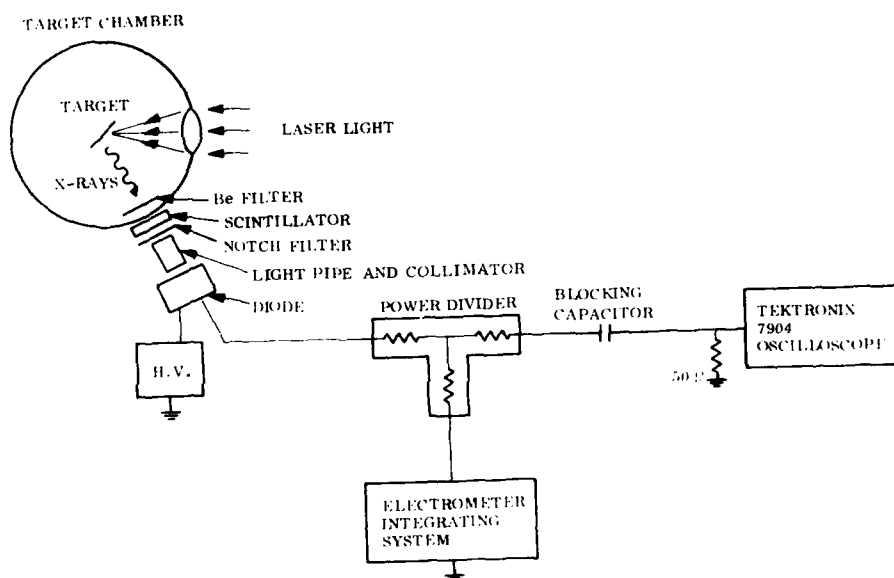
H.V.

50 Ω

ELECTROMETER
INTEGRATING
SYSTEM

Figure 10. Experimental arrangement used for measuring
the ratio of the integral of the short term com-
ponent to the total light as a function of emission
wavelength.

two recording systems. One system recorded the direct "fast" signal by producing a photographic record of the trace on a Tektronix 7904 oscilloscope. Simultaneously, the signal was also directed into an electrometer that integrates the charge for 1 s. Because of the blocking capacitor before the oscilloscope input, the electrometer integrating system eventually collected the total charge delivered by the diode. The scintillator samples (0.32 cm thick by 4.13-cm diameter) were mounted on a special FW114A photodiode package which had a guard-ring structure to prevent any charge leakage. The integrating system and the oscilloscope recording system were both calibrated using the known charge dumped from a "standard" 10-pf capacitor. The oscilloscope time base and voltage deflection were calibrated independently and produced a conversion factor which agreed well with the one obtained from the previously described calibration.

The photographic trace of the FPD signal was digitized and numerically integrated from $t = 0$ to 8 ns. This area was then converted to charge and compared to the total charge collected by the electrometer integrating circuit. For each filter used, five measurements were made and averaged resulting in the data points and standard deviations illustrated in Figure 11.

The filters were bandpass interference filters made by Ditric Optics and were mounted in glass, 2.54 cm square and 0.64 cm thick. They were mounted between the diode and light pipe in an opaque frame that occluded all light paths except that through the filter. The light source was mounted on the opposite end of the 5.1-cm-long lucite light pipe and was apertured to a diameter of 3 cm. The filters had intrinsic bandwidths which varied between 7 and 10 nm (depending on wavelength); however, because of the geometry described above, some light could enter the filter obliquely, thus shifting the center frequency to shorter wavelengths and effectively increasing the total bandwidth. For all cases, the effective bandwidth was estimated to be $\leq$ 20 nm. It is the center frequency of the intrinsic bandwidth that is used in the data plot of Figure 11.
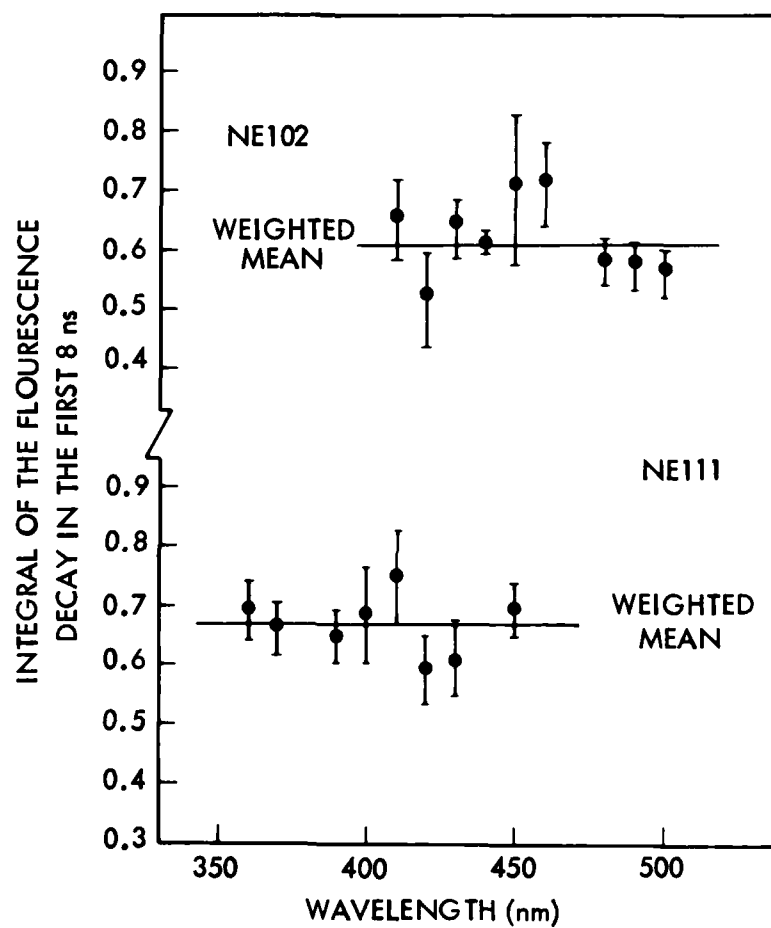
Figure 11. The experimental value of the ratio of the integral of the short term component to the total light integral as a function of emission wavelength.

As illustrated in Figure 11, there appears to be no dramatic change in the ratio of integrals as a function of wavelength. This is also true of the data for NE 102. The solid lines are the weighted means (independent of wavelength) of the data points illustrated. In the case of NE 111, this mean value agrees well with the measured value, for undoped NE 111, obtained in a previous experiment (Ref. 1) in which no selective filtering was employed. For NE 102, the weighted mean is slightly lower than that measured in this earlier experiment (Ref. 1).

Section 4
SATURATION MEASUREMENTS

4.1 INTRODUCTION

Previous studies (Ref. 1) performed at LPARL on the nonlinear, saturation properties of organic scintillators to low-energy x rays were performed at a laser pulse width of 0.2 ns and x-ray energies of $E_x \leq 2$ keV. No nonlinear effects were observed in the response of NE102 and NE111 at irradiances of ≤ 15 mJ/cm^2-ns. These measurements provided the only data available regarding nonlinear effects at high x-ray doses.

The objectives of the present investigation of scintillator nonlinearities were twofold: (1) to continue the studies using 0.2-ns-wide x-ray pulses at irradiances well above the previous limit of 15 mJ/cm^2-ns, and (2), if possible, to study the saturation phenomenon as a function of emission wavelength at pulse widths greater than those previously used. However, because of circumstances it was not possible in the present investigation to complete and include a comprehensive study of this magnitude on a best efforts basis.

The first objective was accomplished and is presented in section 4.2. This information serves as a future reference basis for comparing the response measured as a function of emission wavelength. Although the second objective was not attained in the present study, some data will be included in this report and will serve as a reference basis for any future attempt to measure saturation response as a function of emission wavelength. The data presented in sections 4.3 and 4.4 summarize the results of a recent LPARL investigation (Ref. 5) into nonlinear effects as a function of x-ray pulse width.

4.2 SUBNANOSECOND-PULSE DATA

In principle, the experiment involved the monitoring of changes in scintillator output with respect to systematic changes in x-ray irradiance. This irradiance was

monitored by two detectors positioned at 45 deg to the target on either side of the laser beam. One detector was an x-ray diode (XRD); the other was a scintillator photodiode (NE111 on a ITT FW114). Both the XRD and the scintillator-photodiode monitors were calibrated against a "standard" tantalum foil calorimeter. During the calibration measurements and actual saturation experiment, identical (25.4 μm) beryllium foils were used on all detectors. This use ensured that all detector systems experienced the same incident low-energy spectrum.

The scintillator sample in this experiment was a disk, 0.32 cm thick and 14.3 cm in diameter, of NE111 coupled to an ITT FW114 photodiode through a light pipe and neutral density filter (OD1). The neutral density filter was used in order not to saturate the phototube through space-charge limitation. The purpose of the light pipe was to bring the scintillator (via a special holder through the chamber lid) closer to the target than was previously possible (Ref. 1).

Four factors determined how close the scintillator could be placed to the target: (1) blowoff damage to the beryllium foil, (2) partial occlusion of monitor detectors, (3) introduction of x-ray scattering surfaces that made it difficult to obtain reliable monitor data, and (4) interference with the incoming converging laser pulse. It was found that, at a target spot-to-scintillator distance of 6 mm, any effects due to the above would be avoidable or at a negligible level. However, at distances so close to the target spot, the majority of the x rays would pass obliquely through the beryllium foil covering the scintillator and thus suffer a loss of intensity due to the effective increase in foil thickness. To prevent this loss, a half angle of $\geq$ 18 deg was ensured by fabricating a series of brass collimators (aperture diameters from 0.254 to 1.27 cm) any of which could be placed over the beryllium foil.

The laser pulse energy was held approximately a constant level for these measurements so that no changes in the spectral characteristics would occur. The normal to the target was at 45 deg to the plane formed by the beam and monitor detectors. The scintillator-diode package was positioned above the target at 45 deg to the normal. See Figure 12 for a schematic illustration. The diode package was positioned in a well in the chamber lid so that the scintillator and light pipe could be passed through the base of the well and form a vacuum seal. As was pointed out earlier, the
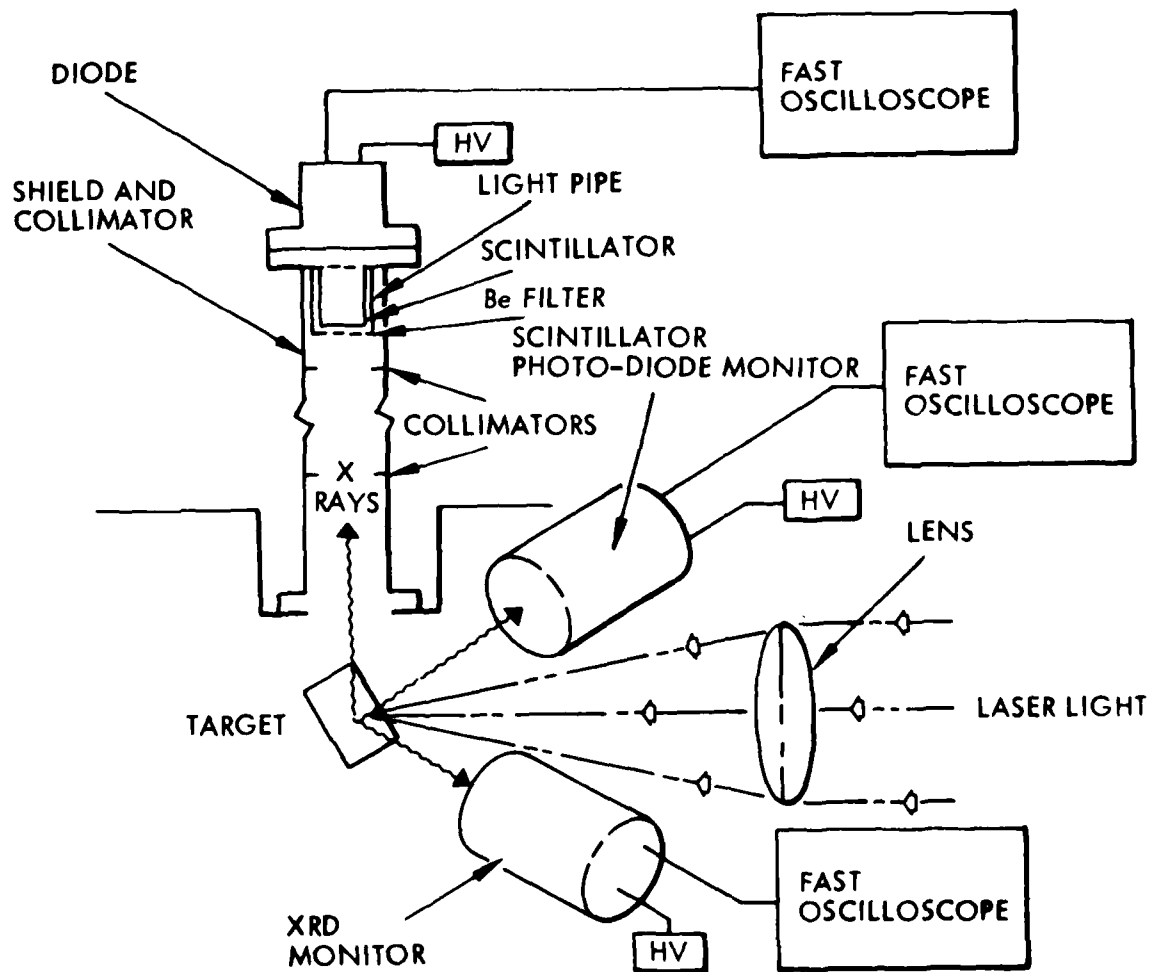
31

Figure 12. Schematic representation of experimental arrangement to be used in the proposed experiment.

closest scintillator-to-target distance was 6 mm. The amount of energy deposited on the surface of the scintillator could be reduced by positioning the diode package at the end of evacuated pipes of different lengths positioned in the well. The actual irradiance experienced by the scintillator was calculated assuming the irradiance varied inversely with the square of the distance from the target.

Detector pulses from the XRD monitor were displayed on a 519 Tektronix oscilloscope and were recorded photographically using Polaroid 410 film. The signals from the sample and monitor photodiodes were recorded in a similar fashion, but 7904 Tektronix oscilloscopes were used. The photographic data were then digitized using TI 980A laser-based computer system and two-dimensional X-Y table. With the use of the appropriate computer program, areas under the digitized waveform could be obtained for the formal analysis.

It was necessary to measure the target-spot-to-scintillator distance quite precisely since a small error at such close distances could be quite serious. With the chamber and detector system under vacuum, the target-spot-to-scintillator distance for the closest gap was measured by viewing the gap through a glass chamber port with a telescope having a calibrated prism translator.

Figure 13 illustrates a plot of waveform areas as a function of x-ray irradiance. The error bars on each data point were estimated to be approximately 10 percent. The solid lines through the data points are a least squares fit to the function

$$y = \sum_0^3 a_k x^k \qquad (1)$$

The test for saturation was based on the search for evidence of a nonlinear relationship between yield and x-ray irradiance. Table 1 lists the resulting expansion coefficients from the least-squares fit to the data.

It is evident from Figure 13 and Table 1 that no gross nonlinearities are present in the data. As terms greater than linear are introduced, no improvement in fit (χ^2)
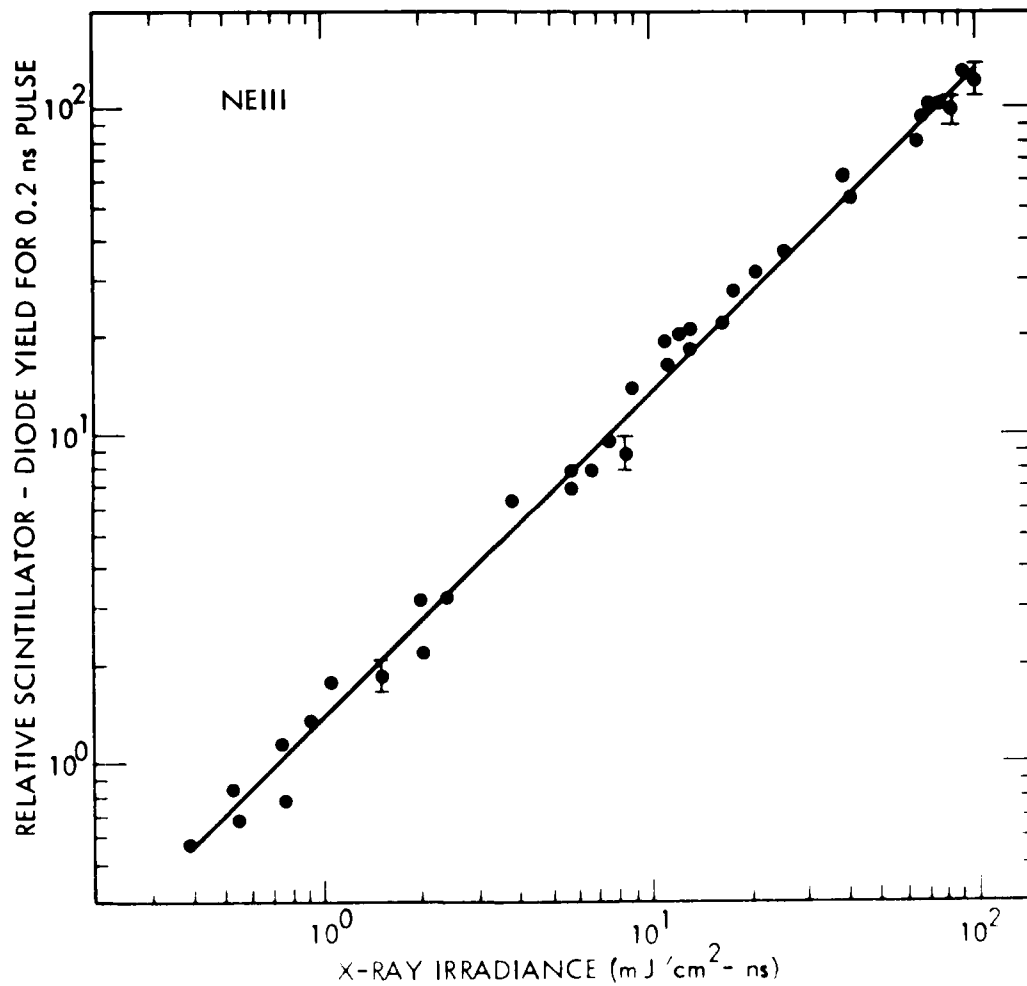
Figure 13. Plot of relative scintillator-diode yield versus x-ray irradiance for a given laser shot. The data are for a 0.2-ns-wide x-ray pulse. Solid lines through the data points are best quadratic fits to data. Experimental error on each datum point is approximately 10 percent.

Table 1. Results of scintillator saturation data analysis based on pulse area.

a_o	a_1	a_2	a_3	χ^2
0.003 ± 0.10	1.36 ± 0.07	(a)	(a)	2.73
-0.003 ± 0.11	1.37 ± 0.10	-0.0003 ± 0.0023	(a)	2.79
0.019 ± 0.13	1.33 ± 0.14	0.0035 ± 0.01	-0.00004 ± 0.00011	2.83

(a) For this case, the a_k coefficient was assumed to be zero.

is attained. In fact, the expansion coefficients, a_o, a_2, and a_3, are in all cases smaller than the associated standard deviation. Since the a_o coefficient is near zero, the implication is that the graph of scintillator output versus irradiance intersects the origin. This is interpreted as strong evidence that no significant nonlinear relation occurs up to the irradiances achieved in this experiment. It is concluded that the 10-percent nonlinearity point lies above 85 mJ/cm^2-ns for a 0.2-ns-wide pulse.

4.3 NANOSECOND-PULSE DATA

In an investigation (Ref. 5) similar to the one presented in section 4.2, the nonlinear effects for nanosecond pulses were studied. To perform studies at longer pulse widths ($\geq$ 1 ns), it was necessary to reconfigure the laser cavity from mode locking to a giant pulse mode. A Pockel cell switching system was set up to switch out prescribed segments of the main giant pulse using charged clipping cables.

The temporal profile of the laser pulse was monitored by a photodiode that detected a small sample of the laser beam reflected from a pellicle positioned just before the entrance to the target chamber. This same detector monitored a sample of the unswitched portion of the laser oscillator pulse. The latter pulse was delayed through an appropriate optical path such that both pulses could be displayed on a single oscilloscope trace. This system provided an online monitor of the laser pulses so that an optimization of the pulse switching system could be maintained and a record provided of the laser beam energy for each shot. A typical laser output with a 7-ns

clipping cable was approximately 10 to 15 J. For a copper target, this output translated into a 6.5-ns-wide burst of x rays at levels up to 10 mJ/sr; at a distance of 0.6 cm from the target, this corresponds to an irradiance of 4.5 mJ/cm^2-ns. Using the appropriate clipping cable, similar irradiances were achieved for a 2-ns-wide x-ray pulse.

Measurements were performed, using a 6.5-ns-wide x-ray pulse, on NE111 and NE102 organic scintillators as well as on NE111 doped with benzophenone, acetophenone, and piperidine. In addition, NE111 was investigated at x-ray pulse widths of 2 and 4 ns. For the NE111 and the doped NE111 measurements, the scintillator on the monitor detector was NE111; for the NE102 sequence, the monitor scintillator was NE102.

To cover a large range of irradiance, a series of different length pipes were available, the longest of which placed the surface of the scintillator at a distance of 148 cm from the target spot. To eliminate the possibilities of x rays being reflected into the scintillator off the walls of the pipes, it was necessary to place apertures of the appropriate diameter in the four longest pipes. Using this system, the scintillator could be exposed to levels of irradiance covering approximately five orders of magnitude.

The NE111 detector system has a time resolution of $\leq$ 1 ns; consequently, it is possible to make an analytical comparison of nonlinear yields as a function of pulse width from data collected at one pulse width. The analysis can be performed by taking data at a long pulse width (e.g., 6.5 ns) and integrating over specific temporal portions of the recorded pulse. In the actual analysis, the 6.5-ns pulse waveforms were integrated over the first 2 ns, the first 4 ns, and the entire 6.5 ns. The half-height point on the leading edge was used as the time reference. Figure 14 illustrates plots of the waveform areas over each of these time regions as a function of x-ray irradiance. Again, the error bars on each data point were estimated to be approximately 10 percent. Table 2 lists the resulting expansion coefficients from the least squares fit of Eq. (1) to the data.

The quality of fit (as indicated by the value of χ^2) does not improve when terms of order higher than $k = 1$ are included in the fit of the 2-ns data. However, in the case of the 4- and 6.5-ns data, the fit quality is improved slightly by the inclusion of
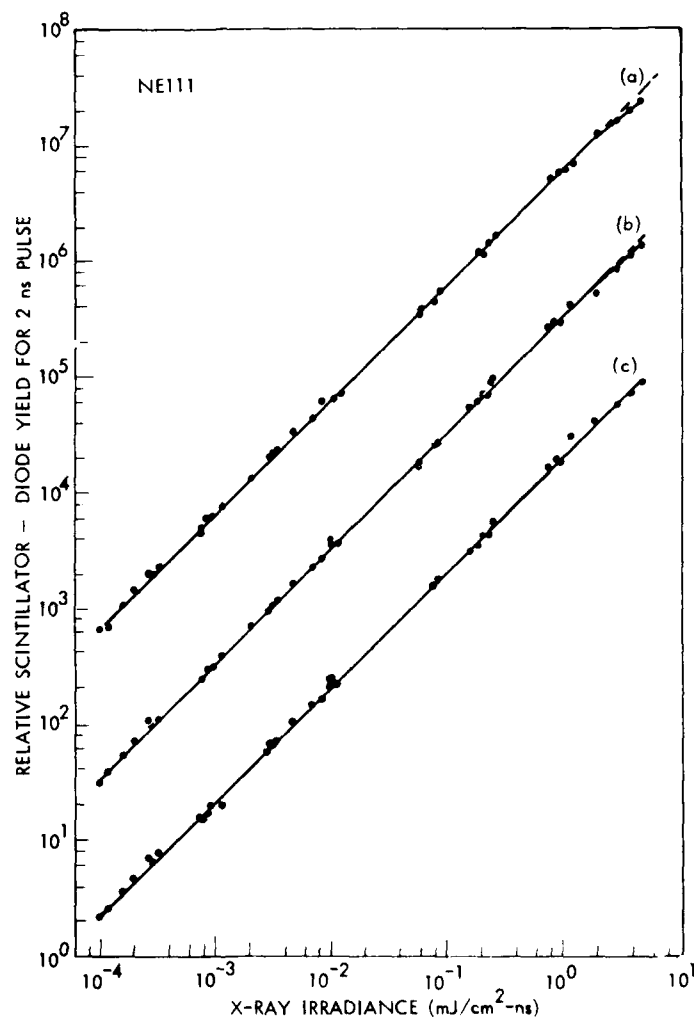
Figure 14. Plot of relative scintillator-diode yield versus x-ray irradiance
for a given laser shot. These data are (a) for a 6.5-ns-wide
x-ray pulse, (b) for the first 4 ns of the 6.5-ns x-ray pulse,
and (c) for the first 2 ns of the 6.5-ns x-ray pulse. Solid lines
through data points are best quadratic fits to data while a dashed
line represents the best linear fit. Experimental error on each
datum point is approximately 10 percent. The vertical axis is
in arbitrary units, and the individual curves are not normalized
to each other.

Table 2. Results of scintillator saturation data analyses using x rays from Cu target and NE111 scintillator.

Pulse Width[a] (ns)	a_0	a_1	a_2	a_3	χ^2
$2^{(b)}$	0.11 ± 0.06	11088 ± 159	(d)	(d)	0.82
	0.09 ± 0.06	11192 ± 176	-170 ± 130	(d)	0.81
	0.11 ± 0.06	11078 ± 186	590 ± 490	191 ± 119	0.79
$4^{(c)}$	0.08 ± 0.10	22162 ± 258	(d)	(d)	0.67
	0.0 ± 0.08	22641 ± 240	-728 ± 172	(d)	0.55
	0.01 ± 0.09	22690 ± 265	-1031 ± 644	77 ± 157	0.55
6.5	0.456 ± 0.224	38329 ± 566	(d)	(d)	0.84
	0.261 ± 0.167	39502 ± 470	-1651 ± 322	(d)	0.61
	0.255 ± 0.175	39536 ± 527	-1839 ± 1242	47 ± 298	0.63

(a) The values of the data points were based on pulse area.
(b) The values of the data points were taken from the first 2 ns of the 6.5-ns data.
(c) The values of the data points were taken from the first 4 ns of the 6.5-ns data.
(d) For this case, the a_k coefficient was assumed to be zero.

higher-order terms. This is particularly true of the 6.5-ns data and is vividly demonstrated in Figure 14 at the highest irradiances. The dashed line is a continuation of the linear fit. In the case of the 4-ns data, this deviation, although present, is not as pronounced as in the case of the 6.5-ns data. The implication is that saturation is occurring at the highest irradiances for the 6.5-ns-wide pulse but not as significantly as for the shorter pulses.

This situation can be evaluated further from the data presented in Figure 15, in which a comparison is made between monitor and signal pulses for three levels of x-ray irradiance. The solid curve is the monitor pulse, while the dashed curve is that of the signal pulse. To make this qualitative comparison, the pulses were normalized to each other by a visual overlay of the leading edges. The waveforms at
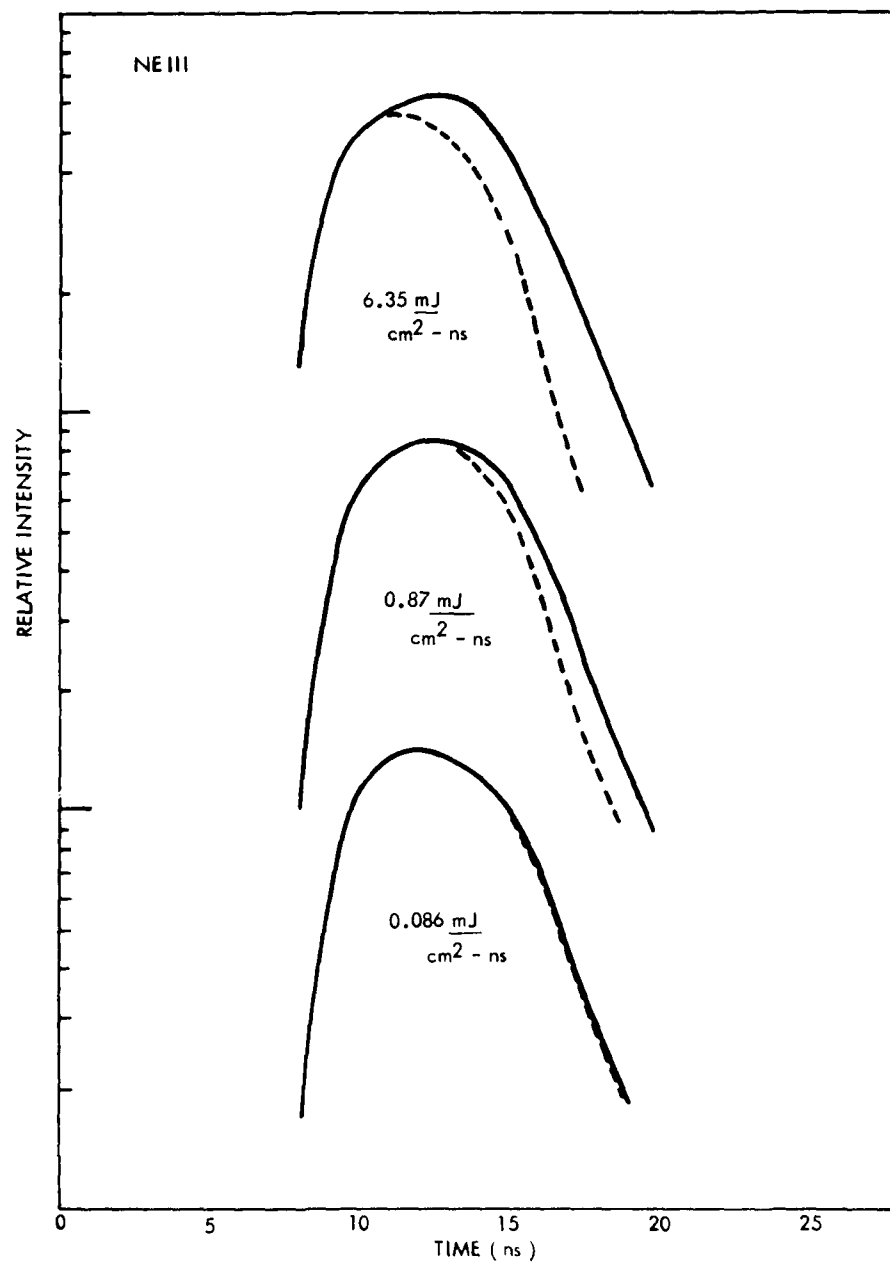
Figure 15. Comparison of shape between monitor and signal scintillator-photodiode pulses for three levels of x-ray irradiance. The solid curve is monitor pulse while dashed curve is signal pulse. The pulses were normalized to each other by visual comparison of the leading edges.

39

6.35 mJ/cm^2-ns were obtained with the scintillator as close as 4 mm. However, as pointed out earlier, data collected that close to the target could not be included in the nonlinearity analysis because of normalization difficulties.

The monitor and signal pulse have similar shapes at the lowest level of irradiance illustrated in Figure 15. For intermediate levels, there appears to be a saturation in the trailing edge of the pulse. At the highest level of irradiance, it appears that a major portion of the pulse undergoes some form of saturation.

Data were collected only at an x-ray pulse width of 6.5 ns for NE102 and doped NE111 samples. The doped samples consisted of 2-, 5-, and 10-percent benzophenone; 5-percent acetophenone; and 10-percent piperidine. These were all similar in shape and size to the undoped NE111 described earlier in this section. As indicated by the studies of NE111, the highest available irradiance would be required to cause saturation; consequently, data were collected mainly at the high end of the available five orders-of-magnitude range in irradiance. Just as in the case of NE111, there was no evidence of nonlinearity except at irradiances above 1 mJ/cm^2-ns.

Since the monitor scintillator was NE111 and not identical to the sample under investigation, a direct comparison between the line shapes of the monitor and the signal FPD could not be made. However, a comparison can be made between signal data taken at low and high irradiances. Figure 16 illustrates scintillator data taken at irradiances of 0.5 and 4.0 mJ/cm^2-ns. The XRD monitor associated with these two laser shots indicated that the temporal profiles of the x-ray pulse were nearly identical. As illustrated in Figure 16, there is obvious distortion in the trailing edge of the pulse taken at the higher irradiance.

4.4 X-RAY DEPOSITION MEASUREMENTS

The x rays emanating from a laser-induced plasma are not monoenergetic. In the case of a Cu target, the spectrum (at the laser energies used in the present investigation) consists of many lines superimposed on a continuum. If one is to analyze the data in terms of an energy dose, it is necessary to characterize the x-ray spectrum well enough so that an average penetration depth for the spectrum can be determined.
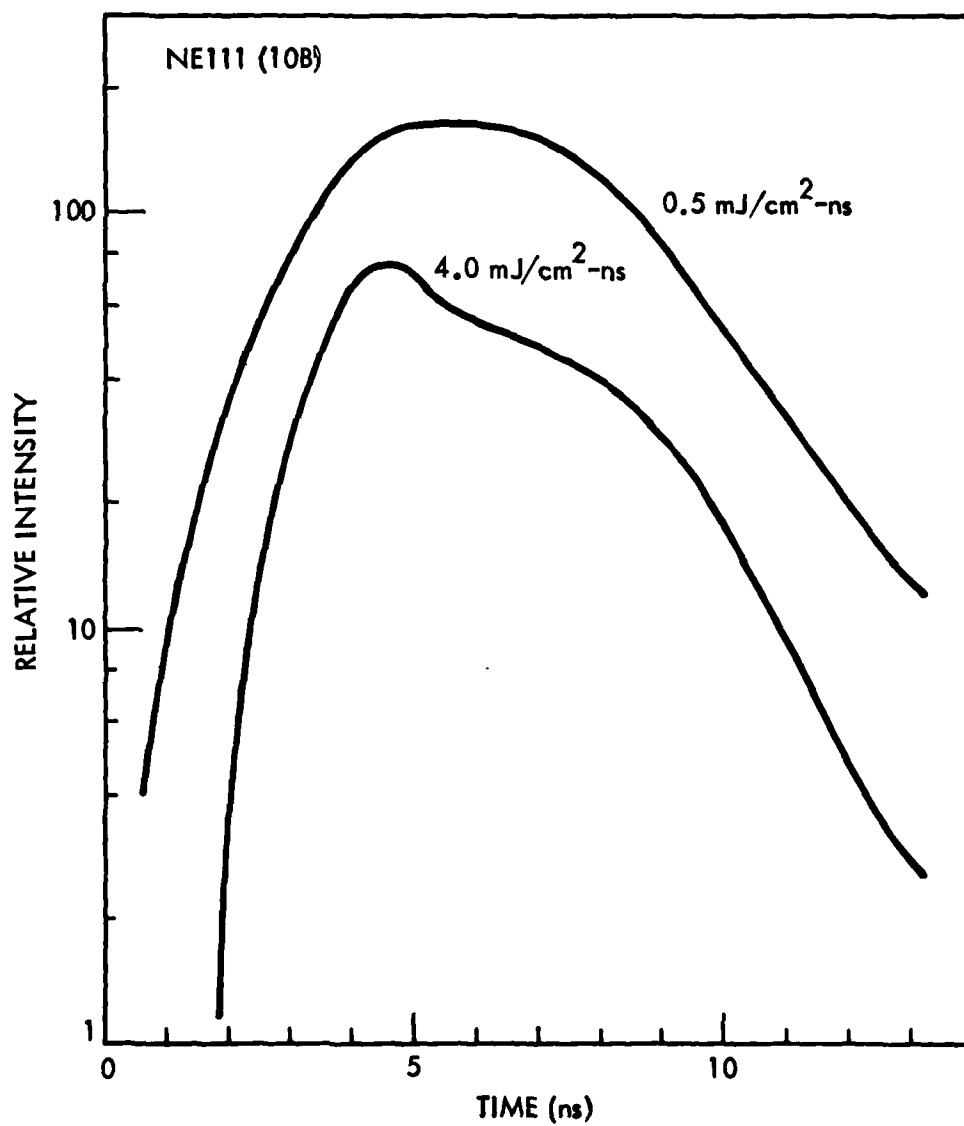
Figure 16. Shapes of two signal scintillator-photodiode pulses taken at
different irradiances. The scintillator is NE111 doped with
10-percent benzophenone. Pulse heights are on a relative
scale and are not normalized to each other.

Such a characterization was performed (Ref. 5) using a spectrometer designed to fit inside the target chamber in a close-coupled geometry. The spectrometer utilized a curved KAP crystal with no screen film. A series of spectra were taken at the laser conditions used in the collection of the nanosecond-pulse saturation data. The spectra were divided into 12 energy bins, and an energy histogram was constructed which contained corrections for film and crystal efficiency as well as all geometrical factors. Utilizing known cross-sectional data, an integration of total energy deposited as a function of depth was performed for the 12 bins in the histogram. The results indicated that 63 percent (one e layer) of the energy was deposited in the first 10 μm of the scintillator. This corresponds to an x ray of energy 1.25 keV and agrees well with the mean energy of the histogram.

Section 5
SUMMARY AND CONCLUSIONS

The emission spectra of doped NE111 were measured and are presented in Section 2. Such spectra were not previously available for the matrix of doped scintillators studied in this and earlier LPARL investigations (Refs. 1 and 5). The results of these measurements indicate that the NE111 emission spectra are composed of at least two major components, one of which usually diminishes in intensity (relative to the other) as the percentage of dopant is increased. Coupling these results with the apparent shift in absorption edge, associated with increasing dopant concentration (section 2.2), one can speculate that a possible mechanism for such a change in spectral shape is that the dopant is acting as an in situ filter.

Since in an earlier LPARL investigation (Ref. 1) the addition of certain doping agents improved the short-term time response, it is tempting to assume that a correlation exists between the disappearance of the short wavelength spectral component and the response improvement. If the doping material is acting as an in situ filter, then it may be possible to produce the same effect with filters external to the NE111 scintillator. If this is the case, it is hoped that the improved response would be attained without the orders of magnitude loss in total light output now experienced when highly doped NE111 is used.

This hypothesis was tested in the experiments described in Section 3. The first of these experiments involved the streak camera to measure the fast-time response as a function of emission spectra wavelength. The results suggested that there is no apparent improvement in fast time response under these conditions. The second experiment was designed to test the possibility of improving the ratio between total light output and that collected in the fast component ($\leq$ 8 ns). The experiment indicated no dramatic change in the long tail component as a function of emission wavelength. This may not be inconsistent with such a simplified interpretation of the doping mechanism,

for it has been shown in previous experiments (Ref. 1) that this ratio is altered by, at most, 17 percent through the use of various dopants and dopant concentrations. It is concluded from the above that the improved response exhibited by the doped NE111 is a manifestation of a far more complex mechanism than the naive interpretation first assumed.

Section 4 presented the results of measurements made in this investigation as well as a previous LPARL investigation (Ref. 5) into the possible nonlinear response of organic scintillators to low-energy x rays. This test was performed over an extensive range of irradiance, approximately five orders of magnitude. No nonlinear response was observed at the highest levels of irradiance ($\sim$ 85 mJ/cm^2-ns) achieved at a pulse width of 0.2 ns. However, a degree of nonlinear response was observed for NE111 at x-ray pulse widths between 6.5 ns and 4 ns and irradiances above 1 mJ/cm^2-ns. The data suggest that at levels below 1 mJ/cm^2-ns, it is safe to assume that for pulses 6.5 ns and shorter, there is no significant level of nonlinearity to x rays with the characteristic spectrum used in these studies.

Based on the collected data, it appears that the level of irradiance for a 10-percent nonlinearity is at approximately 2 mJ/cm^2-ns for a 6.5-ns-wide x-ray pulse. This point lies somewhat higher for a 4 ns-wide pulse and consequently suggests a dose rate as well as total dose dependence. It is unfortunate that higher levels of irradiance could not have been achieved during those studies so that a complete representation of scintillator nonlinearity dependence on pulse width could have been developed.

The apparent discrepancy between the x-ray and electron data (Ref. 2) still exists. Assuming that the nonlinearity effects are dose-rate dependent, the results of the subnanosecond and nanosecond x-ray data presented in this experiment are self-consistent. One possible explanation is that there is a significant deadlayer on the surface of the scintillator that may mask the effects of a low-irradiance nonlinearity. If this deadlayer exists, it is probably an intrinsic property of the scintillator; hence the data presented in this report empirically set the level of nonlinearity for scintillators being used under similar spectral and irradiance conditions.

Calculations based on an average x-ray penetration depth of 10 μm (section 4.4) indicate that the thermal loading of the surface at the highest irradiances is such that the temperature is brought very near the melting point (75°C). This is particularly true in the case of the 0.2 ns-wide-data for which saturation has not yet been observed. In a first-order approximation, the thermal load is $\sim$ 20 J/g and corresponds to an induced surface temperature of $\sim$ 80°C. The corresponding induced surface temperature for the level of irradiance at which nonlinearity was observed for a 6.5-ns-wide-x-ray pulse is $\sim$ 60°C. Ultimately, such a loading may be responsible for a form of transient or permanent surface alteration and thus may be the limiting factor in using scintillators in high-fluence x-ray environments.

REFERENCES

1. Lockheed Palo Alto Research Laboratory, <u>Final Project Officer's Report for Defense Nuclear Agency</u>, DNA 4386-F, Contract DNA001-74-C-0268, Apr 1977

2. J. Stevens and R. B. Knowlen, <u>IEEE Trans. Nucl. Sci.</u>, Vol. 15, 1968, p. 136

3. R. C. Powell and L. A. Harrah, <u>J. of Chem Phys.</u>, Vol. 55, 1971, p. 1878

4. A. F. Lauzon and M. D. Panaro, UOPAD64-15 (1964), unpublished

5. Lockheed Palo Alto Research Laboratory, Final Report for University of California (LLL), LMSC/D630053, Contract PO9451903, Aug 1978

6. Nuclear Enterprises, Inc., "Plastic Scintillators "

<div style="text-align: center">DISTRIBUTION LIST</div>

DEPARTMENT OF DEFENSE

Assistant to the Secretary of Defense
Atomic Energy
        ATTN: Executive Assistant

Defense Technical Information Center
12 cy ATTN: DD

Defense Nuclear Agency
        ATTN: SPTD, W. Summa
        ATTN: DDST
        ATTN: SPTD, T. Kennedy
        ATTN: STRA
 2 cy ATTN: SPTD, R. Webb
 4 cy ATTN: TITL

Field Command
Defense Nuclear Agency
        ATTN: FCTMEI
        ATTN: FCPR
        ATTN: FCTMD
 2 cy ATTN: FCTMOF

Field Command
Defense Nuclear Agency
Livermore Division
        ATTN: FCPRL

Undersecretary of Defense for Rsch. & Engrg.
        ATTN: Strategic & Space Systems (OS)

DEPARTMENT OF THE ARMY

BMD Advanced Technology Center
Department of the Army
        ATTN: ATC-T, M. Capps

Electronics Tech. & Devices Lab.
U.S. Army Electronics R&D Command
        ATTN: DELET-R, S. Kronenberg

Harry Diamond Laboratories
Department of the Army
        ATTN: DELHD-N-P, F. Wimenitz
        ATTN: DELHD-I-TL

U.S. Army Missile R&D Command
        ATTN: Redstone Scientific Info. Ctr.

U.S. Army Nuclear & Chemical Agency
        ATTN: Library

DEPARTMENT OF THE NAVY

Naval Postgraduate School
        ATTN: Code 0142

Naval Research Laboratory
        ATTN: Code 2627

Naval Surface Weapons Center
        ATTN: Code F31

DEPARTMENT OF THE AIR FORCE

Air Force Weapons Laboratory, AFSC
        ATTN: SUL

Deputy Chief of Staff
Research, Development, & Acq.
Department of the Air Force
        ATTN: AFRDQSM

DEPARTMENT OF ENERGY CONTRACTORS

Lawrence Livermore Laboratory
        ATTN: Document Control for Technical
                    Information Dept. Library
        ATTN: Document Control for L-38, H. Reynolds
        ATTN: Document Control for L-203, L. Germain
        ATTN: Document Control for L-21, D. Oakley
        ATTN: Document Control for L-14. W. Dickinson
        ATTN: Document Control for L-200, J. Cortez
        ATTN: Document Control for B. Hudson
        ATTN: Document Control for L-24, O. Vik

Los Alamos Scientific Laboratory
        ATTN: Document Control for P. Whalen
        ATTN: Document Control for MS364
        ATTN: Document Control for P. Lyons
        ATTN: Document Control for R. Thorn
        ATTN: Document Control for C. Keller
        ATTN: Document Control for R. Brownlee
        ATTN: Document Control for H. Agnew

Sandia Laboratories
        ATTN: Document Control for C. Broyles
        ATTN: Document Control for J. Walker
        ATTN: Document Control for 3141
        ATTN: Document Control for J. Plimpton
        ATTN: Document Control for B. Benjamin

DEPARTMENT OF DEFENSE CONTRACTORS

EG&G, Inc.
        ATTN: M. Nelson

General Electric Company-TEMPO
        ATTN: DASIAC

Institute for Defense Analyses
        ATTN: Classified Library

JAYCOR
        ATTN: L. Scott

Kaman Sciences Corp.
        ATTN: F. Shelton

R&D Associates
        ATTN: R. Poll
        ATTN: C. MacDonald
 2 cy ATTN: Technical Information Center

DEPARTMENT OF DEFENSE CONTRACTORS (Continued)

Lockheed Missiles and Space Co., Inc.
    ATTN: D. Kohler
    ATTN: S. Salisbury
    ATTN: R. Bardin
    ATTN: R. Smith
    ATTN: J. Pronko
    ATTN: T. Fisher
2 cy ATTN: L. Chase

DEPARTMENT OF DEFENSE CONTRACTORS (Continued)

Science Applications, Inc.
    ATTN: R. Miller

Systems, Science & Software, Inc.
    ATTN: C. Dismukes